The shape of an elastic filament in a two-dimensional corner flow

Nicolas Autrusson,[1,2] Laura Guglielmini,[2] Sigolene Lecuyer,[3] Roberto Rusconi,[3] and Howard A. Stone[2]
[1]*Supaero, Institut Superieur de l'Aeronautique et de l'Espace, Toulouse 31055, France*
[2]*Department of Mechanical and Aerospace Engineering, Princeton University, Princeton, New Jersey 08544, USA*
[3]*School of Engineering and Applied Sciences, Harvard University, Cambridge, Massachusetts 02138, USA*

(Received 13 September 2010; accepted 28 March 2011; published online 23 June 2011)

The deformation of a flexible filament held fixed at one end in a nonuniform viscous flow with curved streamlines is considered, with a focus on the filament dynamics and steady-state shape. Our motivation arises from recent microfluidic experiments on biofilm formation in a channel with bends, where thread-like structures, or streamers, were observed, attached to the side walls downstream of each corner and connecting consecutive corners while floating in the middle plane of the channel [Rusconi *et al.*, J. R. Soc. Interface 7, 1293 (2010)]. We discuss the time evolution and final shape of the filament in different corner geometries as a function of a non-dimensional elasticity parameter that compares viscous and elastic effects. Since the filament develops tension, when the flow has curved streamlines the filament does not align with the flow, as occurs in a rectilinear flow, but rather it crosses the streamlines. © *2011 American Institute of Physics*. [doi:10.1063/1.3601446]

I. INTRODUCTION

The interplay of viscous and elastic stresses is relevant to a large number of flow problems involving slender elastic fibers. In particular, in low-Reynolds-number flows, elastodynamics is critical to a qualitative and quantitative understanding of the swimming of micro-organisms by wave propagation along an elastic flagella,[1] the motion of elastic filaments driven at their base,[2–4] the design and response of artificial flagella that are activated by external means,[5,6] and the deformation and migration of flexible fibers freely suspended in external flows.[7–13] In this paper, we investigate a variant of these dynamics by studying the evolution and steady shape of flexible filaments fixed at one end in a nonuniform external flow with curved streamlines.

Our motivation for addressing this problem arose from the experimental observation of the formation of biofilm streamers in curved microchannels[14] [see also Figure 7(a) below]. These free-floating, elastic filaments of bacteria and polymer (exopolysaccharides) develop in the flow right after each turn and following the accumulation of biofilms on the walls of the channel. The formation and the development of streamers are strongly related to flow patterns,[15] yet the underlying hydrodynamic mechanisms are worthy of further investigation. We focus here on the shape attained by the streamers floating in the fluid once they had been produced in proximity of a corner or turn.

In order to characterize how slender elastic structures behave in nonuniform flows, in particular of the neighborhood of a corner or turn in a curved channel, we model fluid-structure interactions with slender-body theory.[16] We assume that the flow is two-dimensional and that the filament remains in the plane of the flow. The details of the numerical implementation follow the work of Tornberg and Shelley.[11] An advantage of using this model is its relative simplicity in coupling the filament dynamics to the flow, though we neglect the feedback of the filament on the flow; several studies have extensively used this methods to model dynamics of elastic threads in flow, e.g., Refs. 12 and 17. A similar approach is also presented in Ref. 18, where a shear flow past an array of elastic rods attached to a plane is discussed. In Sec. II, we introduce the approach based on the slender-body theory for the hydrodynamics and the Euler-Bernoulli model for the elastic response of the filament. In addition, we indicate the different boundary conditions used and we discuss the assumptions inherent to the modeling. In Sec. III we present the results of our numerical simulations for the filament dynamics and shape for two different kinds of corners flows, i.e., those with open streamlines and those with regions of closed streamlines. Also, we provide a comparison with the experiments reported by Rusconi *et al.*[14] Lastly, in Sec. IV we outline a theoretical result demonstrating that an elastic filament cannot follow streamlines when the latter are curved.

II. PROBLEM FORMULATION

We consider a slender, inextensible and elastic filament of radius R and length L, with $\epsilon = R/L \ll 1$, suspended in a viscous two-dimensional flow of viscosity μ. We assume external forces, such as gravity and Brownian forces, to be negligible with respect to elastic and viscous forces. We also hypothesize inertial effects to be small, so that the governing equations for the fluid motion are the Stokes equations. Let $\boldsymbol{X}(S,T)$ be the position vector of the filament centerline, where S is the filament arclength and T is the time. The viscous force per unit length $\boldsymbol{F}(S,T)$ exerted on the filament by an undisturbed steady velocity field $\boldsymbol{U}(\boldsymbol{X})$ can be expressed via slender-body theory,[16]

$$\frac{2\pi\mu}{\ln(L/R)}(2\boldsymbol{I} - \boldsymbol{X}_S\boldsymbol{X}_S)\cdot(\boldsymbol{U} - \boldsymbol{X}_T) = \boldsymbol{F}(S,T). \qquad (1)$$

Here, subscripts denote partial derivatives with respect to the independent variables T or S, and capital and lower-case

 © 2011 American Institute of Physics

Downloaded 24 Jun 2011 to 18.84.7.43. Redistribution subject to AIP license or copyright; see http://pof.aip.org/about/rights_and_permissions

characters identify, respectively, dimensional and dimensionless quantities. The anisotropic tensor $(2\boldsymbol{I} - \boldsymbol{X}_S\boldsymbol{X}_S)$ provides the relation between the fluid velocity relative to the filament and the force on the filament. The filament force per unit length $\boldsymbol{F}(S,T)$ consists of bending and tensile contributions; the latter enforces filament inextensibility. These forces can be expressed by the Euler-Bernoulli equation for an elastic beam,

$$\boldsymbol{F}(S,T) = EI\boldsymbol{X}_{SSSS} - (\Sigma(S,T)\boldsymbol{X}_S)_S, \tag{2}$$

where $\Sigma(S,T)$ is the tension in the filament, E is Young's modulus and I is the area moment of inertia about the smallest cross-section of the filament (for a circular cross-section, $I = \pi R^4/4$). The product EI is commonly referred to as the bending modulus. We do not consider any torsion (twist) about the main axis of the filament since the thread is placed in a two-dimensional flow and is assumed to remain with its centerline in the plane of the flow.

We make the problem dimensionless using as length, velocity, and time scales, respectively, the filament length L, a characteristic velocity of the external flow U_0, and the ratio L/U_0. Combining Eqs. (1) and (2), we obtain:

$$\frac{\eta}{2}(2\boldsymbol{I} - \boldsymbol{x}_s\boldsymbol{x}_s)\cdot(\boldsymbol{u} - \boldsymbol{x}_t) = \boldsymbol{x}_{ssss} - (\sigma(s,t)\boldsymbol{x}_s)_s\,. \tag{3}$$

The dimensionless parameter

$$\eta = \frac{4\pi\mu U_0 L^3}{EI\ln(\epsilon^{-1})} \tag{4}$$

represents the ratio of the viscous forces to the elastic forces and characterizes the behavior of an elastic thread immersed in a viscous flow. This ratio is commonly referred to as an effective viscosity,[12] though we prefer to think of it as a dimensionless compliance (η is larger for smaller E). The constraint of inextensibility, which can be expressed as $\boldsymbol{x}_s\cdot\boldsymbol{x}_s = 1$, or equivalently as $\boldsymbol{x}_s\cdot\boldsymbol{x}_{st} = 0$, provides a further condition to be satisfied and yields a second-order boundary value problem for the line tension $\sigma(s,t)$. Thus, using the identities listed in (A1-2), we obtain two coupled partial differential equations for the unknown shape $\boldsymbol{x}(s,t)$ and tension $\sigma(s,t)$ of the filament,

$$\eta(\boldsymbol{u} - \boldsymbol{x}_t) = \boldsymbol{x}_{sssss} - 2\sigma_s\boldsymbol{x}_s - \sigma\boldsymbol{x}_{ss} - 3(\boldsymbol{x}_{ss}\cdot\boldsymbol{x}_{sss})\boldsymbol{x}_s \tag{5a}$$

$$-\eta\boldsymbol{x}_s\cdot\nabla\boldsymbol{u}\cdot\boldsymbol{x}_s = 2\sigma_{ss} - \sigma\boldsymbol{x}_{ss}\cdot\boldsymbol{x}_{ss} + 7\boldsymbol{x}_{ssss}\cdot\boldsymbol{x}_{ss} + 6\boldsymbol{x}_{sss}\cdot\boldsymbol{x}_{sss}. \tag{5b}$$

The problem is closed by appropriate boundary conditions for the filament position and line tension at $s = 0$ and $s = 1$.

We note that Eq. (1) provides the leading-order version of slender-body theory, characterized by an error of magnitude $\mathcal{O}(1/[\ln\epsilon^{-1}]^2)$. This level of approximation is sometimes referred to as a local drag model, since it does not take into account non-local hydrodynamic interactions, such as the fluid-filament interactions or the interactions between the filament and the boundary. For example, Tornberg and Shelley[11] discuss various approaches based on non-local slender-body approximations[19–21] and including the effects of fluid-filament and filament-filament interactions in simulations of highly flexible fibers. For the case of free-filament dynamics, we have compared results from our simulation approach, based on Eqs. (5a) and (5b), with results presented in Ref. 11. For time-dependent deformations, filament position and tension appear nearly identical, when complex dynamics involving non-linear effects such as buckling are not present. Thus, we have not attempted to incorporate higher-order approximations in slender-body theory.

Furthermore, we can take into account filament-wall interactions, when necessary, using an approximation proposed by Katz *et al.*[22] These authors used an integral-equation approach to evaluate the slender-body forces acting on a rigid filament of radius R and length L in motion at a distance H from a planar wall. For $R \ll H \ll L$, the term $\ln(L/R)$ in Eq. (1), or Eq. (4), is replaced by $\ln(H/R)$, in which case $\eta = \frac{4\pi\mu U_0 L^3}{EI\ln(H/R)}$; otherwise the simulations proceed using Eqs. (5a) and (5b), with definition (4) (Fig. 1).

As boundary conditions, while several authors have studied filaments freely suspended in the flow,[2,7,11,12,17] we consider a thread that is held at one end. At the free end, $s = 1$, we require zero force and zero torque, which can be expressed as $\boldsymbol{x}_{ss} = \boldsymbol{x}_{sss} = 0$ and $\sigma(s=1,t) = 0$. At the fixed end, $s = 0$, the filament can be either clamped or hinged.[23] In the first case both the position $\boldsymbol{x}(s=0,t)$ and the slope $\boldsymbol{x}_s(s=0,t)$ of the filament are imposed, i.e., a force of constant orientation is applied at the constraint. In the second case, only the position is imposed and zero torque is applied, so that $\boldsymbol{x}_{ss}(s=0,t) = \boldsymbol{0}$. In both cases we impose $\sigma(s=0,t) = |\int_0^1 \boldsymbol{f}(s)ds|$ because the tension at $s = 0$ has to support the drag force experienced by the filament. With the

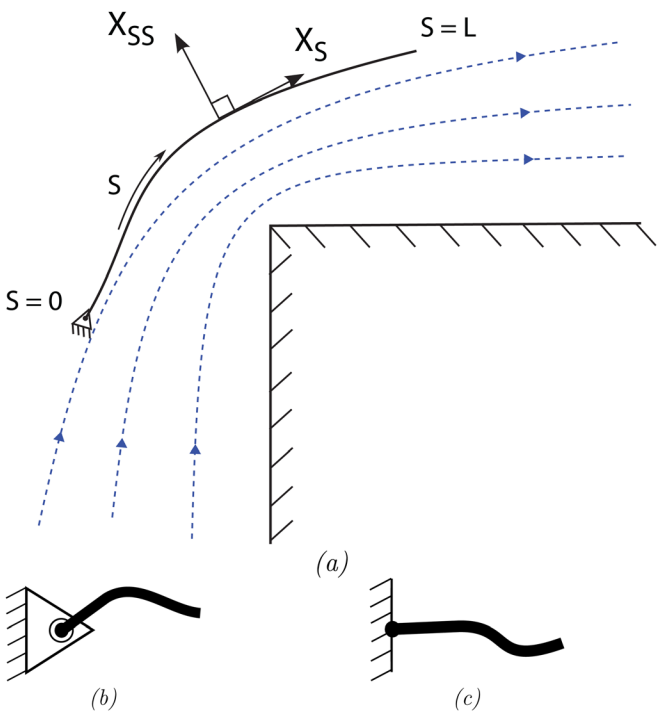

FIG. 1. (Color online) (a) Example of an elastic filament fixed at one end in a low-Reynolds-number flow around a corner. The position of the centerline of the thread is prescribed by $\boldsymbol{X}(S,T)$, with S the curvilinear coordinate. At $S = 0$ the filament can be either (b) hinged or (c) clamped.

Downloaded 24 Jun 2011 to 18.84.7.43. Redistribution subject to AIP license or copyright; see http://pof.aip.org/about/rights_and_permissions

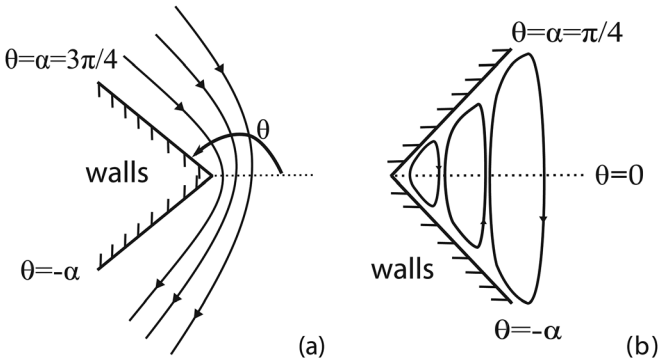

FIG. 2. Viscous flow in the neighborhood of a sharp corner bounded by two infinite walls. Flows antisymmetric in θ: (a) large corner angle ($\alpha = 3\pi/4$), (b) small corner angle ($\alpha = \pi/4$). Streamlines are depicted with arrows to indicate the direction of the flow.

established boundary conditions, the mathematical problem statement is complete.

We solve the differential equations (5a) and (5b) following the numerical approach proposed by Tornberg and Shelley,[11] i.e., we use a second-order backward difference scheme for the time-dependent equation and we treat implicitly only the high-order differences.

III. NUMERICAL RESULTS

We investigate the dynamics of an elastic inextensible filament held fixed at one end in non-uniform flows with curved streamlines, which, to the best of our knowledge, has received limited attention in the literature. The model discussed in Sec. II allows us to study the evolution of the shape of the filament with time until a steady-state is reached and to determine the tension distribution along the filament at each time step. We will show that the steady-state shape of a filament does not follow curved streamlines, but instead intersects the streamlines, which contrasts with the typical behavior in a rectilinear flow.[7] As long as the filament is in a flow with curved streamlines, i.e., the radius of curvature of streamlines is on the order of the filament length or smaller, the thread crosses streamlines.

To illustrate the main ideas, and by analogy with the geometry used in Ref. 14, we study the response of a filament in a Stokes flow in the neighborhood of a sharp corner, the latter being identified by two walls that intersect at an angle 2α (measured through the fluid). In particular, we discuss the cases for $\alpha = 3\pi/4$ and $\alpha = \pi/4$, corresponding, respectively, to flows with open and closed streamlines (Fig. 2).

In the neighborhood of the corner, the two-dimensional viscous flow field is described in cylindrical coordinates (r, θ) by the streamfunction $\psi(r,\theta) = \Re\{\sum f_n(\theta) r^{\lambda_n}\}$, where $\Re$ denotes the real part and λ_n denotes the n th eigenvalue.[24] If we are close enough to the corner, we can consider only the first eigenvalue λ_1, so the streamfunction for an antisymmetric flow reduces to

$$\psi(r,\theta) = A\Re\left\{ r^{\lambda_1}\left(\cos\lambda_1\theta - \frac{\cos\lambda_1\alpha}{\cos(\lambda_1-2)\alpha}\cos(\lambda_1-2)\theta\right)\right\}. \tag{6}$$

The eigenvalue λ_1 is a function of α and for the two cases of interest here, if $\alpha = 3\pi/4$ then $\lambda_1 \approx 1.54$, if $\alpha = \pi/4$ then $\lambda_1 \approx 3.74 + 1.12i$. Moreover, for both configurations we chose the scalar quantity A so that the velocity vector at the base of the filament has unitary modulus, which establishes the velocity scale.

A. Filament in the vicinity of a large corner angle

We now consider the evolution of the thread for $\eta = 100$, i.e., when elastic stresses are small compared to viscous stresses, and we expect large deformations of the thread. In Figure 3, we present the position and the tension of the filament at different times until a stationary solution is established. We established a criterion for the steady state by computing the integral of all of the displacements along the filament between two consecutive time-steps t_n and t_{n+1}, $\ell_n = \int_0^1 \left|\boldsymbol{x}_{(n+1)}(s,t) - \boldsymbol{x}_{(n)}(s,t)\right| \mathrm{d}s$. When $\ell_n < 10^{-6}$, we assume that the steady state has been reached.

The numerical results reported in Figure 3(a) illustrate how the filament deforms and crosses streamlines, as it gets closer to the corner in the downstream direction. Once the steady state is reached, the filament intersects the streamlines near the root ($s=0$) but at the other end ($s=1$) aligns with the almost straight streamlines. The time dependence of the tension in the thread is reported in Figure 3(b), which shows that for all times the tension in the thread is almost linear with arclength, starting from a maximum at $s=0$ and decreasing to zero at $s=1$. It is reasonable that the maximum

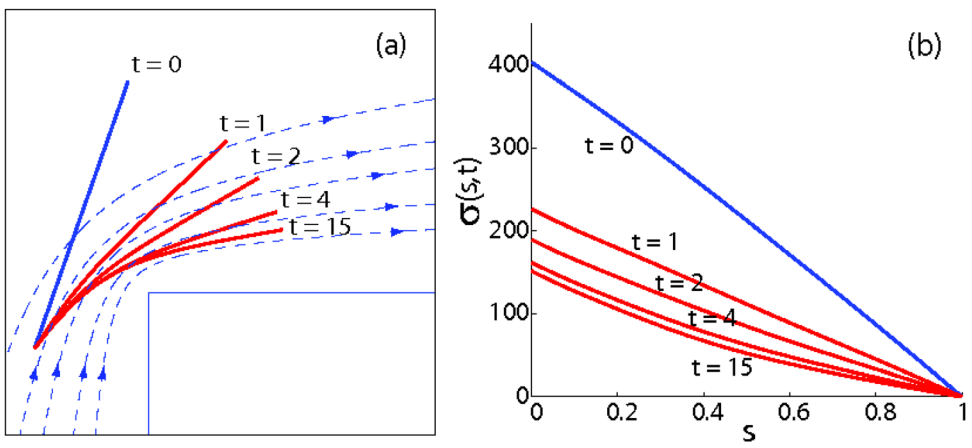

FIG. 3. (Color online) Dynamics of an elastic inextensible filament in the neighborhood of a large corner angle ($\alpha = 3\pi/4$), hinged at $s=0$ and characterized by $\eta = 100$. (a) Position of the thread and (b) tension $\sigma(s,t)$ at different times up to the stationary state ($t = 15$).

Downloaded 24 Jun 2011 to 18.84.7.43. Redistribution subject to AIP license or copyright; see http://pof.aip.org/about/rights_and_permissions

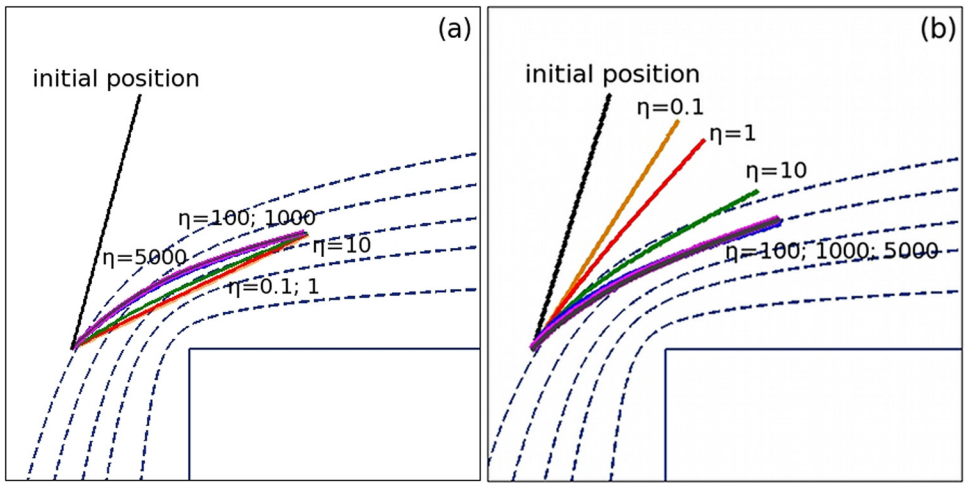

FIG. 4. (Color online) Steady-state position for an elastic filament in the neighborhood of a large corner angle ($\alpha = 3\pi/4$), for different values of $\eta = 0.1, 1, 10, 100, 1000, 5000$. (a) Hinged thread and (b) clamped thread.

tension is at $s = 0$, because the base resists the total drag force experienced by the filament. Furthermore, as time increases, the tension all along the filament decreases. This decrease is rapid between $t = 0$ and $t = 1$, which highlights fast dynamics at the beginning of the simulation. Then, the tension decreases monotonically but at a lower rate until the steady state is established.

We next consider the influence on the steady-state shape of the boundary conditions at the base and of the elasticity parameter η. First, we present the steady-state solution for filaments hinged at $s = 0$ and characterized by different values of η [Figure 4(a)]. Results from similar simulations for filaments that are instead clamped at their base are reported in Figure 4(b). We observe that the steady-state shapes for a hinged or clamped filament are similar as long as the filament is flexible enough ($\eta \geq 100$). For more rigid threads ($\eta = \{0.1, 1, 10\}$), the final configuration of the filament strongly depends on the boundary conditions at $s = 0$. If a hinged end is chosen, then the rigid filament does not deform significantly, but instead it rotates about the base until an equilibrium position is found. For a clamped end, the filament cannot rotate about the root and therefore it bends significantly in the direction of the flow.

B. Filament in the vicinity of a small corner angle

In this section we discuss the dynamics and steady-state shape of an elastic filament suspended in an antisymmetric viscous flow close to a corner with a small internal angle (measured through the fluid). The two-dimensional velocity field is characterized by closed streamlines in the form of an alternating series of counter-rotating vortices centered on the plane $\theta = 0$ (Ref. 24). We discuss the effects of the filament elasticity and position of the base with respect to the center of a selected eddy; the steady state is attained when the condition introduced in Sec. III A is satisfied. We draw the streamlines for one eddy in Figure 5 (recall the length scale is the length of the filament), but note that the theory predicts an infinite sequence of progressively smaller and weaker eddies as the corner is approached.[24]

We first consider the influence of changing the position of the base of the elastic filament for $\eta = 100$. As long as the base is close enough to the center of the eddy [Figure 5(a)], the radius of curvature of the streamlines crossed by the filament is on order of the length of the filament. We observe that the thread rolls up about the center of the eddy. The dynamics is very fast since the steady state is reached for $t = 2$ instead of $t = 15$ (recall the dynamics in Figure 3). We next consider a filament located further from the center of the eddy, where the radius of curvature of the streamlines is large with respect to the filament length. In this case, as the steady state is approached, the second half of the filament tends to align with the streamlines [Figure 5(b)].

Further, for the corner flows we have studied, we verify that changing the initial orientation of the filament does not influence the steady-state shape for the same position of the base of the filament; compare the results shown in Figures 5(b) and 5(c). Because the fluid is rotating in an anti-clockwise direction, the filament in Figure 5(c) undergoes a compressive force at the beginning of the transient state. Since we assumed the thread to be hinged at one end, the thread rotates about the base and bends up to the same final configuration as in Figure 5(b).

Finally, we vary η for the same geometry as in Figure 5(c) by considering a more flexible thread ($\eta = 1000$). Again, the filament first undergoes compression and then aligns with the streamlines. The bending stiffness is not large enough to resist the compressive stresses, so there is a buckling instability which is already observed at $t = 0.1$. Nevertheless, the instability disappears as time increases since the thread is allowed to rotate about its base, and when a steady-state is reached the filament undergoes tension.

In order to complete the characterization of elastic filaments in corner flows with closed streamlines, we determine the final shape of the filament as a function of the dimensionless distance d of the base of the filament from the center of the vortex. Here it is convenient to define the average curvature of the filament $\langle \kappa \rangle = \sqrt{\int_0^1 |\boldsymbol{x}_{ss}|^2 \, ds}$. The dimensionless bending energy per unit length is $\kappa^2(s) = |\boldsymbol{x}_{ss}|^2$. In Figure 6, we plot the average curvature of the filament $\langle \kappa \rangle$ versus the distance d for various values of the effective compliance η. As the base of the filament approaches the center of the eddy, it bends more and its average curvature increases. A larger value of η leads to a higher average curvature of the

Downloaded 24 Jun 2011 to 18.84.7.43. Redistribution subject to AIP license or copyright; see http://pof.aip.org/about/rights_and_permissions

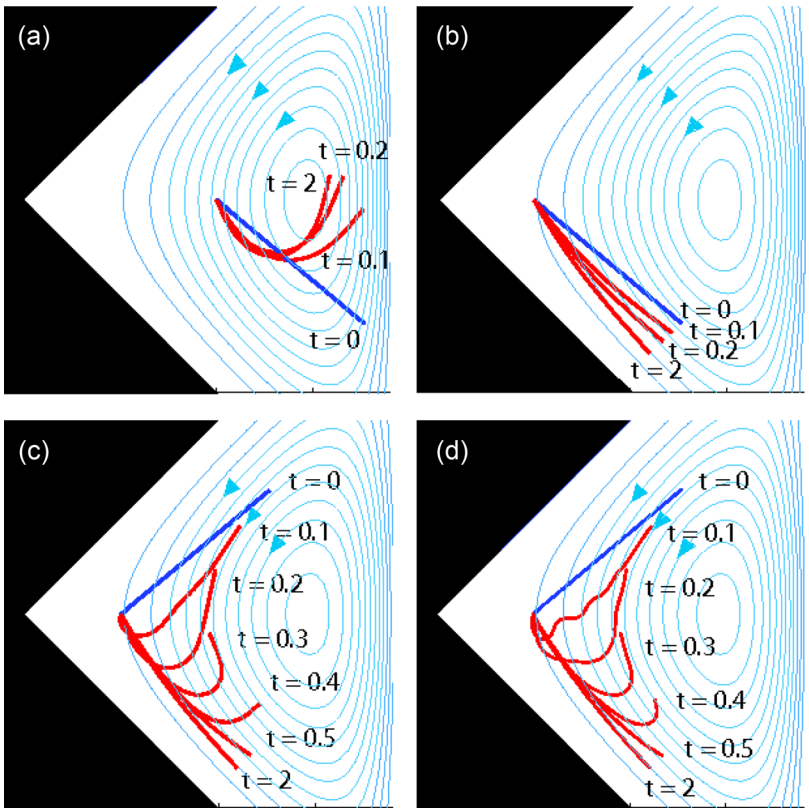

FIG. 5. (Color online) Dynamics of a hinged filament in the neighborhood of a small corner angle ($\alpha = \pi/4$) where the eddy turns in an anti-clockwise direction. For (a) and (b), the filament is characterized by $\eta = 100$ and two different positions of the base. For (c), the filament has a different initial orientation but the base is at the same location of (b). For (d), the filament was made more flexible, $\eta = 1000$.

filament. Furthermore, for all the curves at constant η, we observe a rapid decrease of the average curvature for values of the distance d in the range $0.55 - 0.65$. Therefore, we identify two distinct regimes. When the distance $d \approx 1$, the radius of curvature of streamlines is about the length of the filament, and the filament tends to align with the streamlines [Figure 6(d)]. Hence its bending energy is small and uniform over the filament length [Figure 6(c)]. For values of $d < 0.55$ the filament bends significantly [Figure 6(b)], while its bending energy is large and has a peak in the middle of the filament [Figure 6(a)]. If we further decrease the distance d, the thread tends to roll up about the center of the eddy and its curvature increases at a smaller rate. We did not report results for $d < 0.45$ since the simulations show that the filament continues to roll up with a progressively larger curvature, which violates the assumption made initially in the slender-body equations that the radius of curvature at all points is on the order of the length of the thread.[16]

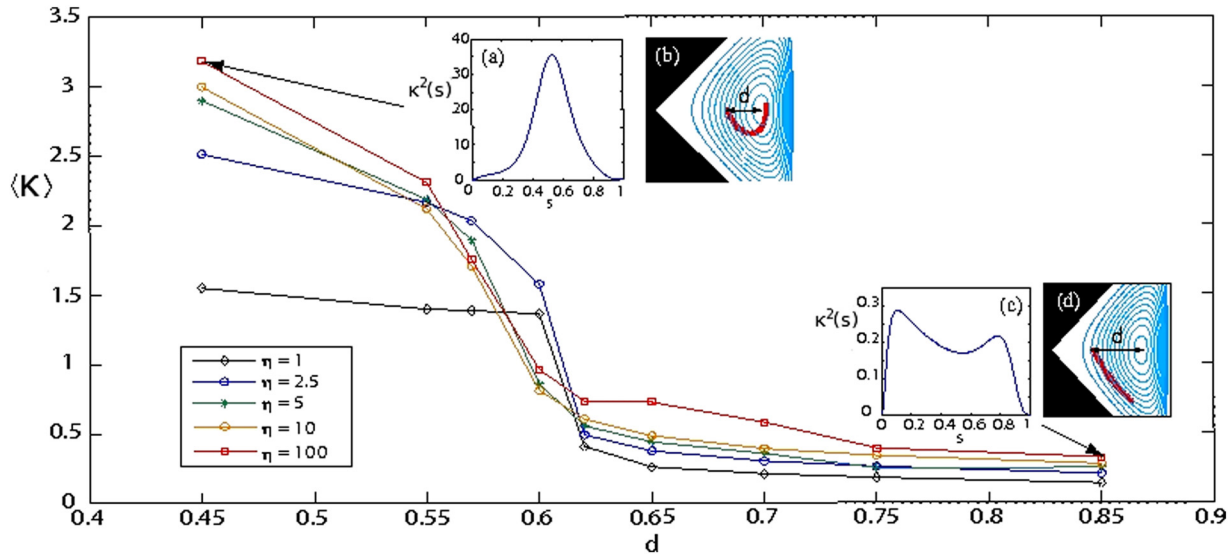

FIG. 6. (Color online) Average curvature $\langle\kappa\rangle$ versus the distance d between the root of the filament and the center of the eddy. Results are presented for various filaments compliances $\eta = 1, 2.5, 5, 10, 100$. Insets: (a) Local bending energy $\kappa^2(s)$ along the filament held close to the vortex center ($d = 0.45$). (c) Local bending energy $\kappa^2(s)$ along the filament held far from the vortex center ($d = 0.85$). The stationary shape of the filament associated with Figures (a) and (c) is presented in Figures (b) and (d), respectively.

Downloaded 24 Jun 2011 to 18.84.7.43. Redistribution subject to AIP license or copyright; see http://pof.aip.org/about/rights_and_permissions

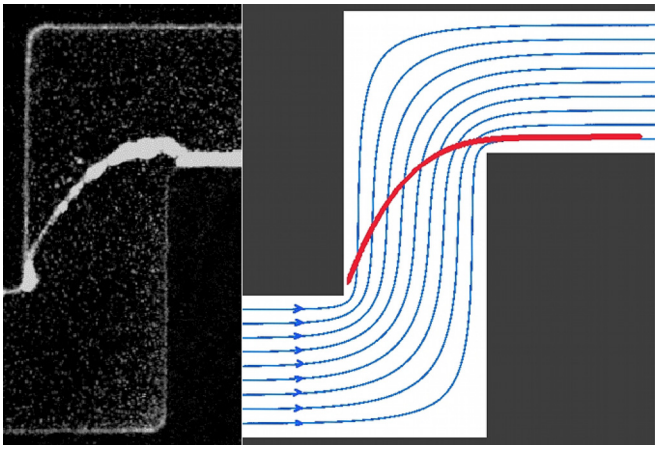

FIG. 7. (Color online) (a) Portion of the channel used in Rusconi *et al.* experiments[14]; streamers with wild-type GFP-labelled PA14 ($OD_{600} = 0.25$) after 12 h of constant flow at 0.75 μl min $^{-1}$. The width of the channel is 200 μm and the height is 100 μm. (b) Simulation for $\mathcal{R}e = 0.006$ and $\eta = 30\,000$. Thin lines refer to the streamlines.

C. Filament in a channel with multiple corners

In this section, we use our slender-body model to study some typical experimental results concerning bacterial streamers. Rusconi *et al.*[14] observed that when a bacterial solution flows in a microfluidic channel at Reynolds numbers $\mathcal{O}(10^{-2})$, a thread-like structure forms everywhere the channel has turns. The continuous filament is attached to the side boundary downstream of each corner, floats in the middle horizontal plane of the channel. In general, the streamer connects consecutive inner corners; one segment of such a streamer is shown in Figure 7(a).

We therefore performed numerical simulations to verify whether our model could reproduce the basic shape of a developed biofilm streamer. For the three-dimensional geometry of Figure 7, the flow field $\boldsymbol{u}$ and the velocity gradient $\nabla \boldsymbol{u}$ that enter Eqs. (5a) and (5b) are not known analytically. Hence, we computed the three-dimensional velocity distribution in a rectangular channel with a bend from direct numerical simulations of the Navier-Stokes equations;[25] numerical simulations using the flow field for a two-dimensional channel with bends yield similar results. In particular, we performed finite-element simulations using Comsol^{TM} software. We then interpolated the quantities of interest at the points describing the position of the thread, i.e., in the middle of the channel, consistently with the experimental results. We used a Reynolds number $\mathcal{R}e = 0.006$ (based on the average speed and the height of the channel) and a compliance $\eta = 30\,000$, to agree with the experimental conditions in Ref. 14. In fact, for this class of experiments it was possible to estimate the elastic properties of the streamer, e.g., for a filament thickness of 10 μm the elastic modulus was estimated as $E = 100$ Pa, a value in the range of what already measured for *P. Aeruginosa* biofilm streamers.[26,27] Moreover, for this problem we use U_0 as velocity scale, the channel flow average velocity.

As shown in the experimental image displayed in Figure 7(a), the filament is connected to the side wall of the channel, a short distance after the first inner corner. According to the physical explanation suggested in,[14] this feature appears to be a consequence of a corner-generated three-dimensional secondary flow characterized by streamwise vorticity and a length scale given by about half the channel thickness.[25] In agreement with experimental observations, we take one end of the filament to be hinged at a fixed point right after the inner corner and on the channel middle plane. We then calculate the steady-state shape of the filament and we observe an excellent match between the experiment and the simulation [see Figure 7(b)]. The numerical streamer crosses streamlines before the corner and the free end becomes tangent to streamlines close to the downstream wall. We have verified that the filament is long enough to ensure that its shape in the region between the two corners is not affected by the length of the filament itself. Our thread-like model however does not reach the wall as in Figure 7(a), which may be a consequence of biological or hydrodynamic interactions between the streamer and polymeric aggregates on the side walls that are not included in our model.

IV. A DEMONSTRATION THAT A FILAMENT DOES NOT FOLLOW CURVED STREAMLINES

In this section we demonstrate that an elastic filament that experiences tension cannot have a steady-state shape that follows the path of curved streamlines. To begin with, we hypothesize that a filament hinged at one end is tangent to the streamlines over its entire length. From Eq. (1), it follows that the drag $\boldsymbol{f}(s)$ is everywhere proportional to the local tangent vector $\boldsymbol{x}_s(s)$. From the inextensibility condition $\boldsymbol{x}_s \cdot \boldsymbol{x}_s = 1$, we then have $\boldsymbol{x}_s \cdot \boldsymbol{x}_{ss} = 0$, so that we can write $\boldsymbol{f}(s) \cdot \boldsymbol{x}_{ss}(s) = 0$. The filament force $\boldsymbol{f}(s)$ can be described via the Euler-Bernoulli model, $\boldsymbol{f} = \boldsymbol{x}_{ssss} - (\sigma \boldsymbol{x}_s)_s$. Hence, we have

$$\boldsymbol{x}_{ssss} \cdot \boldsymbol{x}_{ss} = \sigma(s)|\boldsymbol{x}_{ss}|^2 . \tag{7}$$

We next consider the sign of the tension $\sigma(s)$. Because the filament is held at its base and experiences drag, the tension must be positive over the all entire length of the thread [e.g., Figure 3(b)] and therefore the right-hand side in Eq. (7) is positive for all s. We now integrate the positive quantity $\boldsymbol{x}_{ssss} \cdot \boldsymbol{x}_{ss}$ over the filament length and perform an integration by parts to obtain

$$\int_0^1 \boldsymbol{x}_{ssss} \cdot \boldsymbol{x}_{ss}\, \mathrm{d}s = [\boldsymbol{x}_{sss} \cdot \boldsymbol{x}_{ss}]_0^1 - \int_0^1 |\boldsymbol{x}_{sss}|^2\, \mathrm{d}s. \tag{8}$$

Since the filament is hinged at one end, i.e., $\boldsymbol{x}_{ss}(0) = 0$, and it is free at the other end, i.e., $\boldsymbol{x}_{ss}(1) = 0$ and $\boldsymbol{x}_{sss}(1) = 0$, then

$$\int_0^1 \boldsymbol{x}_{ssss} \cdot \boldsymbol{x}_{ss}\, \mathrm{d}s = -\int_0^1 |\boldsymbol{x}_{sss}|^2\, \mathrm{d}s \le 0 . \tag{9}$$

This conclusion contradicts the sign on the right-hand side of Eq. (7). Therefore, we have demonstrated by contradiction that our initial hypothesis (a filament locally tangent to streamlines over its entire length) must be false i.e., for some s, we must have $\boldsymbol{f}(s) \cdot \boldsymbol{x}_{ss}(s) \neq 0$. Physically, we conclude that a flexible filament cannot follow curved streamlines everywhere, as long as the system is described by the Euler-Bernoulli beam model.

Downloaded 24 Jun 2011 to 18.84.7.43. Redistribution subject to AIP license or copyright; see http://pof.aip.org/about/rights_and_permissions

V. CONCLUSION

In this paper we used slender-body theory for the hydrodynamics and Euler-Bernoulli theory for an inextensible elastic thread to analyze the response of a flexible filament fixed at one end in a nonuniform corner flow. The results underline the importance of the dimensionless compliance parameter η and the type of boundary conditions at the fixed end and illustrate how steady-state shapes cross streamlines of a flow with curved streamlines. The simulations may exhibit buckling when the filament undergoes a strong compression, though, also in those cases, the filament adopts a final steady shape independent of the initial orientation in the flow. Finally, we obtain a good agreement between our approximate numerical model for an elastic filament in a channel flow containing two corners and microfluidic experiments that show a curved bacterial streamer connecting the downstream regions of consecutive corners. These ideas should be useful in other problems involving single or multiple filaments fixed at one end in nonuniform flows.

ACKNOWLEDGMENTS

We thank E. J. Hinch and Y. N. Young for helpful conversations and the BASF Advanced Research Initiative at Harvard University for partial support of the research.

APPENDIX: SOME USEFUL IDENTITIES

Some equalities were helpful to reduce the order of derivatives, and are summarized below.

$$\boldsymbol{x}_s \cdot \boldsymbol{x}_s = 1, \quad \text{from which it follows} \tag{A1a}$$

$$\boldsymbol{x}_s \cdot \boldsymbol{x}_{s,t} = 0 \quad \text{and} \quad \boldsymbol{x}_s \cdot \boldsymbol{x}_{ss} = 0, \tag{A1b}$$

$$\boldsymbol{x}_s \cdot \boldsymbol{x}_{sss} = -\boldsymbol{x}_{ss} \cdot \boldsymbol{x}_{ss}, \tag{A1c}$$

$$\boldsymbol{x}_s \cdot \boldsymbol{x}_{ssss} = -3\boldsymbol{x}_{ss} \cdot \boldsymbol{x}_{sss}, \tag{A1d}$$

$$\boldsymbol{x}_s \cdot \boldsymbol{x}_{sssss} = -4\boldsymbol{x}_{ss} \cdot \boldsymbol{x}_{ssss} - 3\boldsymbol{x}_{sss} \cdot \boldsymbol{x}_{sss}. \tag{A1e}$$

We then find

$$\begin{aligned}
&\boldsymbol{x}_s \cdot \partial_s[(\boldsymbol{x}_s \cdot \boldsymbol{x}_{ssss})\boldsymbol{x}_s] \\
&= \boldsymbol{x}_s \cdot \partial_s[(\boldsymbol{x}_s \cdot \boldsymbol{x}_{ssss})]\boldsymbol{x}_s + \boldsymbol{x}_s \cdot (\boldsymbol{x}_s \cdot \boldsymbol{x}_{ssss})\boldsymbol{x}_{ss} \\
&= \boldsymbol{x}_s \cdot (\boldsymbol{x}_{ss} \cdot \boldsymbol{x}_{ssss})\boldsymbol{x}_s + \boldsymbol{x}_s \cdot (\boldsymbol{x}_s \cdot \boldsymbol{x}_{sssss})\boldsymbol{x}_s + \boldsymbol{x}_s \cdot (\boldsymbol{x}_s \cdot \boldsymbol{x}_{ssss})\boldsymbol{x}_{ss} \\
&= \boldsymbol{x}_s \cdot \boldsymbol{x}_{sssss} + \boldsymbol{x}_{ss} \cdot \boldsymbol{x}_{ssss}.
\end{aligned} \tag{A2}$$

[1]S. F. Goldstein, N. W. Charon, and J. A. Kreiling, " *Borrelia burgdorferi* swims with a planar waveform similar to that of eukaryotic flagella," Proc. Nat. Acad. Sci. U.S.A. **91**, 3433 (1994).
[2]C. H. Wiggins, D. Riveline, A. Ott, and R. E. Goldstein, "Trapping and wiggling: Elastohydrodynamics of driven microfilaments," Biophysical J. **74**, 1043 (1998).
[3]S. A. Koehler and T. R. Powers, "Twirling elastica: Kinks, viscous drag, and torsional stress," Phys. Rev. Lett. **85**, 4827 (2000).
[4]N. Coq, O. du Roure, J. Marthelot, D. Bartolo, and H. Fermigier, "Rotational dynamics of a soft filament: Wrapping transition and propulsive forces," Phys. Fluids **20**, 051703 (2008).
[5]R. Dreyfus, J. Baudry, M. L. Roper, H. A. Stone, and J. Bibette, "Microscopic artificial swimmers," Nature **437**, 862 (2005).
[6]M. Roper, R. Dreyfus, J. Beaudry, M. Fermigier, J. Bibette, and H. A. Stone, "On the dynamics of magnetically driven elastic filaments on the dynamics of magnetically driven elastic filaments," J. Fluid Mech. **554**, 167 (2006)
[7]E. J. Hinch, "The distortion of a flexible inextensible thread in a shearing flow," J. Fluid Mech. **74**, 317 (1976).
[8]P. O. Brunn, "Hydrodynamically induced cross stream migration of dissolved macromolecules (modelled as nonlinearly elastic dumbbells)," Int. J. Multiphase Flow **9**, 187 (1983).
[9]R. E. Goldstein and S. A. Langer, "Nonlinear dynamics of stiff polymers," Phys. Rev. Lett. **75**, 1094 (1995).
[10]L. C. Nitsche, "Cross-stream migration of bead-spring polymers in nonrectilinear pore flows," AIChE J. **42**, 613 (1996).
[11]A. K. Tornberg and M. J. Shelley, "Simulating the dynamics and interactions of flexible fibers in Stokes flows," J. Comp. Phys. **196**, 8 (2004).
[12]Y. N. Young and M. J. Shelley, "Stretch-coil transition and transport of fibers in cellulars flows," Phys. Rev. Lett. **99**, 058303 (2007).
[13]E. Wandersman, N. Quennouz, M. Fermigier, A. Lindner, and O. du Roure, "Buckled in translation," Soft Matter **6**, 5715 (2010).
[14]R. Rusconi, S. Lecuyer, L. Guglielmini, and H. A. Stone, "Laminar flow around corners triggers the formation of biofilm streamers," J. R. Soc., Interface **7**, 1293 (2010).
[15]R. Rusconi, S. Lecuyer, N. Autrusson, L. Guglielmini, and H. A. Stone, "Secondary flow as a mechanism for biofilm streamers formation," Biophys. J. **100**, 1392 (2011).
[16]R. G. Cox, "The motion of long slender bodies in a viscous fluid. Part 1. General theory," J. Fluid Mech. **44**, 791 (1970).
[17]L. E. Becker and M. J. Shelley, "Instability of elastic filaments in shear flow yields first-normal stress differences," Phys. Rev. Lett. **87**, 198301 (2001).
[18]C. Pozrikidis, "Shear flow past slender elastic rods attached to a plane," Int. J. Solids Struct. **48**, 137 (2011).
[19]T. Gotz, "Interactions of fibers and flow: Asymptotics, theory and numerics," Ph.D. Thesis (University of Kaiserslautern, Germany, 2000).
[20]R. E. Johnson, "An improved slender-body theory for slow viscous flow," J. Fluid Mech. **99**, 411 (1980).
[21]J. Keller and S. Rubinow, "Slender-body theory for slow viscous flow," J. Fluid Mech. **75**, 705 (1976).
[22]D. F. Katz, J. R. Blake, and S. L. Paveri-Fontana, "On the movement of slender bodies near plane boundaries at low Reynolds number," J. Fluid Mech. **72**, 529 (1975).
[23]S. M. Han, H. Benaroya, and T. Wei, "Dynamics of transversely vibrating beams using four engineering theories," J. Sound Vib. **225**, 935 (1999).
[24]H. K. Moffatt, "Viscous and resistive eddies near a sharp corner," J. Fluid Mech. **18**, 1 (1964).
[25]L. Guglielmini, R. Rusconi, S. Lecuyer, and H. A. Stone, "Three-dimensional features in low-Reynolds-number confined corner flows," J. Fluid Mech. **668**, 33 (2011).
[26]P. Stoodley, Z. Lewandowski, J. D. Boyle, and H. M. Lappin-Scott, "Structural deformation of bacterial biofilms caused by short-term fluctuations in fluid shear: An in situ investigation of biofilm rheology," Biotechnol. Bioeng. **65**, 84 (1999).
[27]N. Aravas and C. S. Laspidou, "On the calculation of the elastic modulus of a biofilm streamer," Biotechnol. Bioeng. **101**, 196 (2008).

Downloaded 24 Jun 2011 to 18.84.7.43. Redistribution subject to AIP license or copyright; see http://pof.aip.org/about/rights_and_permissions